The Organization of Frontostriatal Brain Wiring in Non-Affective Early Psychosis Compared with Healthy Subjects Using a Novel Diffusion Imaging Fiber Cluster Analysis

James Levitt (james_levitt@hms.harvard.edu)
Harvard University
Fan Zhang
https://orcid.org/0000-0002-5032-6039
Mark Vangel
Paul Nestor
Yogesh Rathi
Suheyla Cetin-Karayumak
Brigham and Women's Hospital and Harvard Medical School https://orcid.org/0000-0002-3315-5821
Marek Kubicki
Brigham and Women's Hospital, Harvard Medical School https://orcid.org/0000-0002-3989-8212
Michael Coleman
Kathryn Lewandowski
McLean Hospital/Harvard Medical School https://orcid.org/0000-0003-1477-6187
Daphne Holt
Matcheri Keshavan
Beth Israel Deaconess Medical Center https://orcid.org/0000-0002-5945-888X
Dost Ongur
dongur@partners.org
Alan Breier
Martha Shenton
Harward/BWH
Lauren O'Donnell
Harvard Medical School Brigham and Women's Hospital. https://orcid.org/0000-0003-0197-7801

Article

Keywords: Diffusion Magnetic Resonance Imaging, Tractography, Brain Wiring, Prefrontal Cortex, Caudate

Posted Date: September 20th, 2022

DOI: https://doi.org/10.21203/rs.3.rs-2062646/v1

Version of Record: A version of this preprint was published at Molecular Psychiatry on May 12th, 2023.
See the published version at https://doi.org/10.1038/s41380-023-02031-0.

Abstract

Background

Alterations in brain connectivity may underlie neuropsychiatric conditions such as schizophrenia. We here assessed the degree of convergence of frontostriatal fiber projections in 56 young adult healthy controls (HCs) and 108 matched Early Psychosis-Non-Affective patients (EP-NAs) using our novel fiber cluster analysis of whole brain diffusion magnetic resonance imaging tractography.

Methods

Using whole brain tractography and our fiber clustering methodology on harmonized diffusion magnetic resonance imaging data from the Human Connectome Project for Early Psychosis we identified 17 white matter fiber clusters that connect frontal cortex (FC) and caudate (Cd) per hemisphere in each group. To quantify the degree of convergence and, hence, topographical relationship of these fiber clusters, we measured the inter-cluster mean distances between the endpoints of the fiber clusters at the level of the FC and of the Cd, respectively.

Results

We found 1) in both groups, bilaterally, a non-linear relationship, yielding convex curves, between FC and Cd distances for FC-Cd connecting fiber clusters, driven by a cluster projecting from inferior frontal gyrus; however, in the right hemisphere, the convex curve was more flattened in EP-NAs; 2) that cluster pairs in the right ($p = 0.03$), but not left ($p = 0.13$), hemisphere were significantly more convergent in HCs vs EP-NAs; 3) in both groups, bilaterally, similar clusters projected significantly convergently to the Cd; and, 4) a significant group by fiber cluster pair interaction for 2 right hemisphere fiber clusters (numbers 5, 11; $p = .00023$; $p = .00023$) originating in selective PFC subregions.

Conclusions

In both groups, we found the FC-Cd wiring pattern deviated from a strictly topographic relationship and that similar clusters projected significantly more convergently to the Cd. Interestingly, we also found a significantly more convergent pattern of connectivity in HCs in the right hemisphere and that 2 clusters from PFC subregions in the right hemisphere significantly differed in their pattern of connectivity between groups.

Introduction

In this study, we assess frontostriatal structural connectivity (i.e., brain wiring) in early psychosis non-affective (EP-NA) subjects. Frontostriatal connectivity is the initial component of frontrostriatal circuitry,

which modulates functions that are abnormal in schizophrenia such as executive functions e.g., [1]. Diffusion magnetic resonance imaging (dMRI) tractography [2–5] allows for an *in vivo* method to measure the local variation in brain connectivity patterns in human subjects. Here, we have applied dMRI tractography in a novel manner to investigate putative structural connectivity disturbances (brain miswiring) in frontostriatal connections in early psychosis patients. We have previously published normative data about brain wiring in frontostriatal connectivity [6] using this approach and here apply it in early psychosis subjects where the confounds of medication and chronicity are relatively small. In addition, as brain wiring is formed during early development [7], the presence of its altered pattern in adult subjects lends support to developmental hypotheses of schizophrenia [8–11]. Further, measures of brain miswiring in schizophrenia could serve as developmental biological markers to identify those early psychosis patients who might benefit from early intervention.

Schizophrenia (SZ) is a psychotic disorder which manifests both positive and negative symptoms such as hallucinations, delusions and avolition, as well as prominent cognitive abnormalities including impaired executive function. It is thought to be associated with disrupted white matter connectivity between brain regions e.g., [12,13]. Based on the evidence of abnormal brain functional connectivity in SZ e.g., [14,15], it is important also to examine brain structural connectivity. The primary focus of this paper, the frontostriatal circuit, modulates higher cognitive functions and behaviors, including executive function and goal directed behavior, which are core clinical deficits in schizophrenia [1,16,17].

The striatum is the main input nucleus of the basal ganglia for cortical projections and channels feedback to the cortex, via the thalamus, through the output nuclei of the basal ganglia [18,19]. A topographic, tripartite, functional organization of the striatum with limbic, associative and sensorimotor subloops has been described [20]. Corticostriatal projections, which contain frontostriatal circuits, have a generally topographic, functionally segregated, anatomic organization [18]. However, non-topographic, functionally integrative cortical projections, which anatomically overlap at the level of the striatum, also exist [19,21]. Animal tract tracing and human imaging studies [19,21–23] both support the existence of corticostriatal projection patterns yielding integrative and segregated corticostriatal target zones. The function of striatal target zones that receive overlapping cortical projections is to allow for integration of information from different cortical functional subregions [19,24].

Prior studies have used dMRI to assess frontostriatal white matter pathways in humans with developmental brain disorders. Such studies have shown reduced fractional anisotropy (FA) in attention deficit hyperactivity disorder (ADHD) in right frontostriatal projections [25,26], increased fiber density in fragile X syndrome in left ventral frontostriatal tracts [27] and increased FA with decreased RD in multiple frontostriatal tracts in 22q11.2 deletion syndrome [28]. In a prior study in first-episode schizophrenia patients using dMRI tractography, we showed a reduction in FA in several frontostriatal tracts, and in one of these tracts, a reduction in FA was correlated with impaired executive function [29]. In addition, in our prior studies of chronic schizophrenia, using dMRI tractography to assess diffusion measures and

connectivity wiring patterns, we showed reduced FA as well as reduced streamline counts in frontostriatal circuitry [17]. In a subsequent dMRI tractography study, using a different approach to evaluate brain wiring, we assessed the degree of overlap in frontal projections to the striatum and showed a less integrative pattern of connectivity in chronic schizophrenia vs healthy controls (HCs) [30].

Using our current fiber clustering methodology in a prior study [6], we assessed HC subjects to establish a normal wiring pattern which can later be contrasted with other neuropsychiatric conditions. We showed that the normative PFC wiring pattern projecting from the PFC to the caudate, deviates from a strictly topographic, parallel, organization, due to a pattern of convergence in regionally specific anatomic fiber clusters connecting the PFC and striatum. We found that these clusters originated in subregions in the ventrolateral, dorsolateral and orbitofrontal PFC.

In the current study, we compared the frontostriatal wiring pattern in EP-NA subjects with that of HC subjects. We employed our novel way of using tractography using a fiber clustering method [31]. This approach utilizes machine learning to generate clusters of streamlines, or fibers, based on the similarity of their trajectories. With this approach, we identified and analyzed all fiber clusters connecting regions of interest (ROIs) in the frontal cortex and the caudate for their degree of geometric convergence. More specifically, to assess the geometry of the input from multiple fiber clusters, we measured the mean distance between the endpoints of streamlines of fiber clusters at the level of frontal cortex (i.e., cortical distance) and the mean distance between the endpoints of the corresponding streamlines of fiber clusters at the level of the caudate (i.e., caudate distance; see **Fig. 1.**).

Based on animal work e.g., [21] and our prior human work [6, 30], we hypothesized 1) frontostriatal connectivity in both groups would show a pattern of deviation from a strictly anatomically topographic arrangement with selective PFC subregions showing greater convergence; 2) certain clusters in both groups would show greater patterns of convergence coming from subregions of the frontal cortex, which we surmise may subserve functions that benefit from greater circuit integration; and, 3) HCs would show a more convergent FC-caudate connectivity pattern compared to EP-NA subjects.

Methods

Subjects

This study was comprised of data from 108 young adult EP-NA subjects and 56 controls from the Human Connectome Project for Early Psychosis (HCP-EP) (MPI: Shenton, Breier). Subjects were recruited from 4 HCP-EP sites (Indiana University, Massachusetts General Hospital, McLean Hospital and Beth Israel Deaconess Medical Center-Massachusetts Mental Health Center). MRI data were acquired from 3 HCP-EP sites, 1 in Indiana, 1 at Brigham and Women's Hospital (with subjects from McLean, Massachusetts General Hospital, and Beth Israel Deaconess Medical Center-Massachusetts Mental Health Center) and later MRI data were also acquired at McLean Hospital.

Image Acquisition and preprocessing

The HCP-EP dMRI data were acquired using a modified HCP-Lifespan protocol to cut down on the overall time in the scanner (https://www.ncbi.nlm.nih.gov/pmc/articles/PMC6649668/) A 3 T Prisma Siemens Prisma scanner was used and images were processed using a well-designed pipeline (https://github.com/pnlbwh) that included motion correction, eddy current correction and EPI distortion correction. The acquisition parameters were: TE = 89.2ms, TR = 3230ms, partial fourier of 6/8, multi-band factor of 4 and voxel size = 1.5x1.5x1.5 mm^3. Data were acquired along 206 gradients in both AP and PA phase encoding directions at b-values of b = 500, 1500 and 3000 s/mm^2 with 6 gradient directions at b = 500 s/mm2 and 100 gradients along each of b = 1500 and 3000.

Structural Image post-processing

Diffusion Imaging Data Harmonization

The dMRI data were harmonized using our harmonization methodology [32] (https://github.com/pnlbwh/dMRIharmonization). Briefly, data were acquired from four different sites, and dMRI data were acquired on a 3T Siemens Prisma scanner from two (Brigham and Women's Hospital, Indiana University) and then a third scanner was added (McLean Hospital). Control subjects from each site were used to learn a mapping between the sites, with the BWH used as the reference site. Data from all other sites were then harmonized to the BWH site. As shown in [32], post-harmonization, the statistical differences due to scanner effects were removed.

Diffusion Imaging Two-tensor whole brain tractography post-processing

In the harmonized dMRI data, whole brain tractography was computed using a two-tensor model Unscented Kalman Filter (UKF) method [33, 34] that accounts for crossing fibers, as implemented in the *ukftractography* package (https://github.com/pnlbwh/ukftractography). A two-tensor model was chosen to account for the many crossing fibers [35, 36] found in the architecturally complex white matter tracts. The two-tensor model associates the first tensor with the main direction of the fiber tract that is being traced, while the second tensor represents fibers crossing through the tract. The UKF method is highly consistent in tracking fibers using dMRI data from independently acquired populations across ages, health conditions and image acquisitions [31], and it is more sensitive than standard single-tensor tractography [37–39]. Visual and quantitative quality control of the tractography was performed using the quality control tool in the *whitematteranalysis* (WMA) software (https://github.com/SlicerDMRI/whitematteranalysis).We extracted the b = 3000 shell of 92 gradient directions and the single b = 0 scan for each subject, as applied in our previous studies that perform tractography-based analysis using HCP data [31, 40–42]. Angular resolution is better and more accurate at high b-values such as 3000 [43, 44] and this single shell was chosen for reasonable computation time and memory use when performing tractography. Specifically, tractography was seeded in all voxels within the

brain mask where FA was greater than 0.1. Tracking stopped where the FA value fell below 0.08 or the normalized mean signal (the sum of the normalized signal across all gradient directions which was employed to robustly distinguish between white/gray matter and cerebrospinal fluid) fell below 0.06, as recommended for HCP data in [31]. Fibers that were longer than 40 mm were retained to avoid any bias towards implausible short fibers [45–47]. For each of the subjects under study, there were about 700,000 fibers in the whole brain tractography.

Fiber clustering methods

Cluster analysis

To enable the identification of fiber tract parcels (i.e., fiber clusters) from orbital, lateral and medial prefrontal cortical regions projecting to the caudate, we used a data-driven fiber clustering atlas [31]. This atlas allows for a whole brain tractography parcellation into 2000 fiber clusters according to the white matter anatomy (i.e., fiber geometric trajectory). The clusters themselves were comprised of fibers, or streamlines, that reflect the trajectory of white matter axons (See **Fig. 1.**).

In brief, the atlas was generated by creating dense tractography maps of 100 individual HCP subjects (an independent population from the HCP subjects used in the present study) and then applying a fiber clustering method to group the tracts across subjects according to their similarity in shape and location. For each cluster in the atlas, the tract anatomical profile (TAP) [31], i.e. the set of segmented brain FreeSurfer regions through which the cluster passed, is provided. The TAP was calculated based on the 100 HCP-atlas subjects, as described in [31]. Briefly, for each cluster, the set of intersected FreeSurfer regions per atlas subject was computed. Then, the set of regions (here, a given ROI in the PFC and the caudate) intersected by at least 40% of fiber streamlines of this cluster across all atlas subjects was used to define the cluster's TAP. In this work, fiber clusters of interest from the cortex projecting to the caudate were identified according to their connected anatomical brain regions as defined in the TAP, in the same way as used in our previous study [6]. In this way, we identified 17 white matter fiber clusters that connected the PFC and the caudate in both left and right hemispheres. The following FreeSurfer ROIs [48] were used to identify the clusters of interest to generate the streamlines of interest: the caudalanteriorcingulate, caudalmiddlefrontal, lateralorbitofrontal, medialorbitofrontal, parsopercularis, parsorbitalis, parstriangularis, rostralanteriorcingulate, rostralmiddlefrontal, superiorfrontal, frontalpole cortical ROIs and the caudate nucleus.

Inter-cluster streamline endpoint distance analysis

To quantify the topographical relationship of these fiber clusters, we used our strategy of inter-cluster endpoint distance analysis [6]. To achieve this, between each pair of fiber clusters we measured the mean Euclidean distance between the endpoints of streamlines at the level of the frontal cortex (i.e., the cortical inter-cluster, pairwise, end point distance) and the mean Euclidean distances between the endpoints of the streamlines in the corresponding fiber cluster pair at the level of the caudate (i.e., the caudate inter-cluster, pairwise, endpoint distance; see **Fig. 1.)**. This, in turn, allowed us to quantify the degree of

convergence or divergence, i.e., deviation from a parallel, strictly topographic organization, among the 17 frontostriatal fiber cluster projections.

Statistical Analysis

To determine the pattern of frontostriatal connectivity in both groups, first, we generated scatter plots for each hemisphere (see **Fig. S1.**) based on the 17 fiber clusters (with 136 pairs of fiber clusters, yielding 136 data points), that showed the relationship between the cortical distances and the corresponding caudate distances of the fiber cluster pairs that connect the prefrontal cortex and the caudate. An exponential model describing the connectivity pattern was then fit to the data points as previously shown in Levitt et al. [6]. Second, in both groups, we generated scatter plots (see **Fig. S1.**) for each of the 17 clusters. For each cluster in each group, we performed a paired t-test of the distance from that cluster to the other clusters in the hemisphere, comparing these mean inter-cluster streamline endpoint distances at the level of the frontal cortex and at the level of the caudate, adjusting for the 17 tests performed, per hemisphere, using a Bonferroni correction.

Third, we categorized the mean differences in cluster endpoint distances (EP-NA minus HC) between groups in each hemisphere and plotted them with a convex hull (i.e., the smallest convex polygon containing all of the data points in the plot) yielding 4 quadrants with the point of origin signifying no group difference (see **Fig. 2.A.**). We used the signs of the differences of the endpoint distances in Cd and FC for each cluster pair for the 4 quadrants to calculate the number of cluster pairs in each quadrant (++; +-; -+; – quadrants) for both hemispheres. We tested the null hypothesis for each hemisphere, using chi-square analysis, that the number of data points would not differ among the 4 quadrants. We used chi-square tests for each hemisphere, with p-values determined by permutation, to test quadrant location of the mean difference in cluster pair endpoint distances (EP-NAs minus HCs) between groups. See **Fig. 2.B.** which shows an example of how 2 cluster-pairs (2 blue; 2 brown lines) one with a relatively more divergent pattern from an EP NA subject (blue line), and one with a relatively more convergent pattern (brown line) from a HC, when subtracting endpoint distances, will result in point location in the upper left quadrant in **Fig. 2.A.**.

Lastly, we assessed the between-group difference for each cluster pair in each cluster in the degree of convergence, reflected by a convergence quotient (CQ). Our CQ was calculated as: (Cortex $_{Distance}$ - Caudate $_{Distance}$)/ (Cortex $_{Distance}$ + Caudate $_{Distance}$). For each cluster, we employed a mixed model regression analysis of the degree of cluster pair convergence, i.e., the cluster pair CQs, in both left and right hemispheres separately.

Results

Subject Demographics

164 young adult subjects were included in this study from the Human Connectome-EP project including 108 EP-NA subjects (73.:1% males; 26.9% females) and 56 HCs (66:1% males; 33.9% females) $X^2_{(1,164)}$ = 0.89, p = 0.34). EP-NA subjects mean age was 22.5 ± 3.5; HC subjects mean age was 23.8 ± 4.0 ($t=_{(1,162)}$; p = 0.03). EP-NA subjects mean age was 23.8 ± 4.0; HC subjects mean age was 22.5 ± 3.5 ($t=_{(1,162)}$; p = 0.03). For Full scale IQ, EP-NA (n = 106) subjects had a mean score = 99.3 ± .16.6; HC subjects (n = 55) had a mean score = 115.4 ± 11 for EP-NA ($t=_{(1,149.4)}$7.1; p < .001). See Table 1 for further demographic information including cognitive measures, duration of illness, chlorpromazine (CPZ)-equivalents, educational level, clinical measures, and diagnostic subtypes.

The overall pattern of frontostriatal connectivity

For both groups in both hemispheres, to evaluate the overall pattern of connectivity between the FC and striatum, we generated scatter plots in each hemisphere (see **Fig. 3.A.**). These plots were based on the 17 fiber clusters per hemisphere (with 136 pairs of fiber clusters, yielding 136 data points) that connect the FC and the caudate. These scatter plots show the relationship between the cortical cluster endpoint distances at the level of the cortex and corresponding cluster endpoint distances at the level of the caudate for each of the 136 fiber cluster pairs. We fit an exponential model to the data points which proved to be superior to a linear model for both groups in both hemispheres (see **Fig. 3.A.**).

We found a non-linear relationship between inter-cluster cortical distances and caudate distances in both HCs and EP-NA groups in both left and right hemispheres which was driven by the results from the same 10 cluster pairs highlighted by the green circles located in on the right lower portion of the scatter plot [below] the exponential curve in **Fig. 3.A.**. In **Fig. 3.A.**., the 16 green circles represent clusters that include cluster number 6 as one its cluster pairs. Of note, a cluster originating in the inferior frontal gyrus, pars triangularis, fiber cluster number 6, was significantly over-represented in these 10 cluster pairs as can be seen by its being a member of each of these 10 cluster pairs for both groups in both hemispheres. Of further note, we found that the correlation curve in the right hemisphere showed a qualitatively different, and more flattened, non-linear relationship in the EP-NA patient group vs HCs, visually suggesting that the wiring pattern in the RH differed between groups (see **Fig. 3.A. (d)**).

Cluster variation in the pattern of frontostriatal connectivity

To determine the local variation of the pattern of frontostriatal connectivity in both left and right hemispheres, in both groups, we generated scatter plots for each of the 17 cluster pairs that show the relationship between cortical and caudate endpoint distances between that cluster and the other 16 (See **Fig. S1.**). Paired t-tests comparing the mean inter-cluster endpoint distances in cortex and caudate between each cluster with the other 16 clusters in each group, revealed that for both groups fiber clusters coming from the ventrolateral (clusters 6, 8 in LH and RH), rostral middle frontal gyrus (cluster 1 in the RH), medial and lateral orbital frontal cortex, (cluster 10 in LH and RH) showed significant convergence (i.e., caudate endpoint distance < cortex endpoint distance) after correcting for multiple tests (adjusted p value < 0.05**).** See Supplementary **Table 2.** for the t-test p-values for fiber clusters showing significant

patterns of frontostriatal convergence. See **Fig. 3.B.** for the scatter plot of cluster 6 and see **Fig. S1.** for the scatter plots of all fiber clusters. We note that **Fig. 3.B.** showing the scatter plots of cluster pairs that include cluster 6 as one of the cluster pairs, represent the same data points as the green circles in **Fig. 3.A. (a), (b), (c)**, and **(d)**.

Group comparison of the degree of convergence in frontostriatal connectivity

We used two between group approaches to quantify the group difference in frontostriatal connectivity reflected in the difference in the fitted curves that we observed in the right hemisphere shown in **Fig. 3.A.**. First, we categorized the group mean difference in cluster endpoint distances in both FC and Cd areas by subtracting the HC distances from the EP-NA distances between groups in each hemisphere. We, in turn, used the signs of the differences of the endpoint distances in Cd and FC for each cluster pair, and demonstrated that there was a significantly greater number of cluster pairs with positive Cd and negative FC differences in the RH, but not in the LH. See **Fig. 2.A.** showing a plot enclosed by a convex hull perimeter with cluster pair 5, highlighted in red, against a background of all cluster pairs represented by the black plus signs. Also, see **Fig. 2.B.** visually demonstrating how we calculated the plot quadrant locations (++; +-; -+; – quadrants) for each group difference in endpoint distances. Then, using a chi-square test with p-values determined by permutation, we showed for these pairwise cluster comparisons that there was an overall more convergent pattern in HCs compared with EP-NAs in the right (RH p = 0.03) but not left (LH p = 0.13) hemisphere (see **Fig. S2.**).

Second, using a mixed model regression analysis of the degree of cluster pair convergence, i.e., the cluster pair CQs, for both left and right hemisphere separately, we showed a significant group by fiber cluster pair interaction for 2 RH fiber clusters. These fiber clusters were numbers 5 and 11, which withstood significance correction for the 17 clusters in each hemisphere (p = .00023; p = .00023). See **Fig. 4.**. (See **Fig. S3.** for similar plots of each cluster in both hemispheres). We note that fiber cluster number 5 originates in the frontal pole and the rostral middle frontal gyrus (rMFG), and fiber cluster number 11 originates in rMFG and inferior frontal gyrus (IFG), pars orbitalis (see **Fig. 5.**).

Discussion

In this study we used our novel diffusion imaging fiber cluster tractography method to assess the organization of frontostriatal brain wiring in EP-NA subjects and in HCs. We had four major findings. First, we found that the overall F-Cd wiring pattern, bilaterally, in both HCs and EP-NAs, deviated from a strictly topographic organization primarily driven by a cluster from IFG, pars triangularis. This was shown by non-linear, convex curves between inter-cluster cortical distances and caudate distances driven by the results from 10 cluster pairs in the left (LH) and right hemispheres (RH) in both HCs and in EP-NAs, all of which included a cluster coming from IFG, pars triangularis. Of note, however, we found a group difference such that in the RH in EP-NAs, the convex curve was more flattened. Second, for both groups in both hemispheres, we found certain clusters that showed significantly greater cluster pair convergence.

More specifically, we found FC-caudate cluster projections with significantly more convergent patterns originating from PFC ventrolateral, dorsolateral, and orbitofrontal subregions Third, we found a more convergent FC caudate wiring pattern in the RH in HCs compared to EP NAs. More specifically, we showed that there was a greater number of FC-caudate cluster pairs with a more convergent projection pattern in HCs vs EP-NA subjects which was significant in the right, but not left, hemisphere. Fourth, we showed a significant group by fiber cluster pair interaction for 2 right hemisphere fiber clusters projecting from the frontal pole and rostral middle frontal gyrus (cluster 5) and from rostral middle frontal gyrus and inferior frontal gyrus, pars orbitalis (cluster 11), respectively.

Our finding showing a bilateral pattern of more localized deviation from a general topographic pattern of connectivity between the FC and caudate is both a replication and an extension of our prior study in healthy subjects (Levitt, 2021). We conclude that such an anatomical pattern of connectivity is generally present in human brains and thus might be considered a transdiagnostic feature of brain organization. Further, we surmise that regions that deviate from a strictly topographic pattern of connectivity (i.e., either increased or decreased convergence), add greater circuit complexity and both promote greater cross-talk and circuit integration at the level of the striatum. Despite some similarities between groups in connectivity patterns between frontal cortex and caudate, our findings also importantly suggest group differences in the degree of convergence of such connectivity, what we call the CQ score, which occur both at an overall level of organization as well as at a more localized level. Specifically, we find in pairwise comparisons of all 136 clusters that more clusters in HCs are convergent in HCs than in EP-NAs which is significant in the right hemisphere. Also, we find that cluster 5, coming from the frontal pole and rostral middle frontal gyrus and the contiguous cluster 11, coming from the right hemisphere inferior frontal gyrus, pars orbitalis and rostral middle frontal gyrus, are the 2 localized subregions of the PFC whose patterns of projecting streamlines, with all other clusters, differ between EP-NA and HC subjects. Such specific clusters can be conceived of as specific subcircuits within the total PFC-caudate circuitry. Our method, thus, allows for a highly refined way of measuring localized brain wiring deviations from a healthy control pattern. These FC regions and the subcircuits projecting from them, as discussed below, subserve higher cognitive functions, such as executive functions, impaired in schizophrenia.

Our finding is novel as it isolates a specific brain circuit (the FC-caudate loop within the cortico-basal ganglia circuitry) and demonstrates using dMRI tractography in *vivo* group differences between EP-NA subjects and HCs. Such a finding is consistent with current thoughts that SZ is caused by dysconnectivity in brain circuits. For example, multiple studies have shown that functional and structural connectivity is disrupted in SZ [14, 15, 17, 49].

As brain wiring occurs early in development, its disruption comports well with a neurodevelopmental hypothesis of schizophrenia e.g., [8, 11, 50]. Further, as macroscale (i.e., long tract) brain wiring is established developmentally and then is enduring [51], dMRI tractography measures of brain wiring should serve as strong candidate trait biomarkers for disorders such as SZ with abnormal brain wiring e.g., [30]. Moreover, genes affecting neuronal migration and axonal growth which can disrupt white matter long

tract brain connectivity, have been found to be associated with schizophrenia [52, 53]. Further, prenatal stress, a risk factor for SZ, as shown in a non-mammalian vertebrate model via maternal immune activation, can influence circuit formation and normal axonal development [54].

With regard to prefrontostriatal brain wiring development in non-human primates, autoradiographic tract tracing studies in monkeys have shown a distinct pattern of corticostriatal connectivity that is established in the final third of pregnancy prior to birth [51]. Importantly, this pattern can be shown in newborn monkeys as well as in adult monkeys [55]. More specifically, it has been shown that PFC-Cd fibers terminate in a pattern in which terminals are concentrated in patches surrounded by areas without PFC input, described as fenestrated by Goldman [55], and that a transformation from a diffuse pattern of distribution during early gestation to a fenestrated pattern occurs by the final third of pregnancy [51, see Fig. 6].. As adult monkeys continue to show the fenestrated pattern [55], the above strongly implies that in monkeys after the fenestrated pattern emerges during the final third of pregnancy, it persists into adulthood. Thus, the above monkey data suggest that our finding of group difference in FC-Caudate wiring patterns between HCP-EP subjects and HCs reflects wiring patterns that emerged prenatally and persisted throughout postnatal development into adulthood.

The organization of corticostriatal anatomic connectivity has been thoroughly investigated through the use of animal tract tracing studies and in human brain imaging studies [22, 30, 56]. Animal tract tracing studies have shown projection zone overlap in the striatum of cortical projections e..g., [21, 57, 58]. For example, in a more recent monkey tract tracing study, Averbeck et al., [21], found the pattern of corticostriatal connectivity deviated from a strictly topographic one. They compared the distance between pairs of injection sites in the frontal cortex in monkeys with the degree of overlap in the projection zones of these cortical injection sites. They found an exponential decrease in overlap in striatal projection zones as a function of greater distance between pairs of injection sites. Such non-human primate studies suggest that projection zone overlap is a characteristic anatomic feature of corticostriatal connectivity. In healthy human subjects, Draganski et al. [22], using probabilistic diffusion imaging, reported projection zone overlap in the striatum coming from prefrontal, premotor and motor cortices. Although our data do not determine where fibers terminate inside the striatum, we interpret our convergence measures to reflect a pattern of projection convergence from the prefrontal cortex to the caudate as similar to a pattern of projection zone overlap described by Averbeck et al. [21] and Dranganski et al. [22].

The cortico-basal ganglia circuitry has been described to influence a number of important higher cognitive functions, in addition to its traditional role in influencing motor activity. As our data shows clusters 5 and 11 in the right hemisphere differentiate groups, it is of interest to review the function of the subregions from which these clusters project, i.e., the frontal pole, and rMFG (cluster 5), and the rMFG and lFG, pars orbitalis (cluster 11).

The rMFG is located in the dorsolateral PFC. It is a critical component of the frontoparietal control network and subserves processes that include goal directed behavior, cognitive flexibility, such as mental

set shifting, and working memory e.g., [20, 59, 60, 61]. The IFG has been shown to be engaged by word retrieval and the updating of working memory [62]. In addition, the IFG, in particular in the right hemisphere, has been shown to subserve inhibitory control. For example, damage to the right hemisphere IFG in human subjects and rodents has been shown to interfere with inhibitory control [63–65]. Further, the frontal pole has been described as involved in cognitive functions including multi-tasking, prospective memory, and mentalizing (i.e., theory of mind), functions which have been subsumed under the term metacognition e.g., [65, 66]. Deficits in such functions might cause significant difficulties in social cognition and employability, skills deficient in patients with schizophrenia e.g., [67, 68]. Of note, impairments in the above higher cognitive functions have been described in schizophrenia [1, 29, 69–72].

Limitations of the paper include that the design of the study is a cross-sectional one. The idea that our brain wiring measures reflect normal neurodevelopment and its deviations should be confirmed in longitudinal studies across the lifespan. Other limitations include that medication and illness chronicity confounds cannot be ruled out as many of the patients were receiving antipsychotics and illness durations were variable. A further potential limitation is that individual streamlines within fiber clusters need not terminate directly onto the caudate in order to be counted in the endpoint calculations as described above in the Methods section. Lastly, we acknowledge the risk of false negative and false positive streamlines using dMRI tractography e.g., [73, 74]. For future studies, it will be important to apply these measures in subjects over the lifespan, from early childhood to old age, to test their stability. Further, we plan to explore this circuitry in other neuropsychiatric disorders, such as early psychosis affective subjects, and to explore sex as a potential variable affecting brain wiring. Finally, FC-caudate brain wiring behavioral associations should also be explored.

In summary, employing a novel use of dMRI tractography, we found for both HCs and EP-NAs that the overall FC-caudate wiring pattern similarly deviated from a strictly topographic relationship and had similar clusters that projected to the caudate in a significantly convergent pattern of connectivity. Conversely, we found an overall significantly more convergent pattern of connectivity in HCs in the right hemisphere and that 2 specific clusters from selective PFC subregions in the right hemisphere significantly differed in their pattern of connectivity between HC and EP-NAs. We surmise that regions showing group differences impact certain higher cognitive functions disrupted in schizophrenia including cognitive control, inhibition and metacognition. Lastly, we believe the importance of our brain wiring measures is that they reflect trait biomarkers which can help to identify subjects with schizophrenia, early in their development, who would benefit from early treatment intervention.

Table 1. Demographic, Neuropsychological and Clinical measures

	EP-NA Subjects (N = 108)[a]		HC Subjects (N = 56)[a]					
	Mean	SD	Mean	SD	df	t-test	χ^2	p-value
Age (years)	22.5	3.5	23.8	4.0	1, 162	2.24		0.03*
Males/Females	79/29		37/19		1,164		0.89	0.34
FSIQ[b]	98.8 (n = 106)	16.6 (n = 106)	115.4 (n = 55)	11.0 (n = 55)	1, 156.4	7.51		< 0.001**
Vocabulary T Score[c]	51.27 (n = 106)	12.54 (n = 106)	60.27 (n = 55)	8.79 (n = 55)	1,145.77	5.27		< 0.001**
Duration of illness (days)	652.22 (n = 104)	466.66 (n = 104)	NA					
Antipsychotic Medication Dosage (CPZ equivalent for lifetime reported as mg/day)[d]	323.75 (n = 84)	209.68 (n = 84)	NA					
Education level 1[e]	n = 24		n = 2			NA		
Education level 2[f]	n = 77		n = 24			NA		
Education level 3[g]	n = 5		n = 22			NA		
Education level 4[h]	n = 2		n = 8			NA		
PANNS Positive Marder[i]	15.45 (n = 103)	4.54	NA			NA		
PANNS Negative Marder[j]	12.97 (n = 101)	5.18						
DSMV-TR Diagnosis subtype: schizophrenia	n = 56		NA					

Table 1. Demographic, Neuropsychological and Clinical measures		
DSMV-TR Diagnosis subtype: schizoaffective	n = 20	NA
DSMV-TR Diagnosis subtype: schizophreniform	n = 8	NA
DSMV-TR Diagnosis subtype: Other psychoses[k]	n = 7	
[a]The sample size (n) differs among variables owing to unavailability of data in some participants. [b]FSIQ= Composite Score Estimate (based on Wechsler Abbreviated Scale of Intelligence – second Edition (WAS-II)). [c]Vocabulary T Score (based on (WASI-II) [d]79 Patients received neuroleptic medication (lifetime); 5 patients received no neuroleptic medication (lifetime). No data was unavailable for 24 subjects. [e]Education level 1: <High School Degree; [f]Education level 2: High School degree, GED, Associates Degree or Some University Courses; [g]Education level 3: Bachelor's degree, Some Graduate level courses, Doctoral level courses; [h]Education level 4: Completed an advanced degree (Master's Degree and beyond). [i]PANSS Positive Marder - Positive and Negative Syndrome Scale with Marder Factors [75]. [j]PANSS Negative Marder - Positive and Negative Syndrome Scale with Marder Factors. [k]Other psychoses include other specified psychosis, delusional disorder, brief psychotic disorder. NA = data not applicable. CPZ = Chlorpromazine. DSMV-TR = Diagnostic and Statistical Manual of Mental Disorder, Fifth Edition, Text Revised. DSMV-TR subtype data was unavailable for 17 subjects.		
*p < 0.05, **P < 0.001		

Declarations

Grant Support: R21MH121704 (Levitt); U01MH104977 (PIs: Shenton, Breier, Ongur, Holt, Keshavan); R01MH119222 (PIs: Rathi, O'Donnell); R01MH125860 (PIs: O'Donnell, Rathi, Makris); P41EB015902 (PI: Kikinis, Westin), R01MH074794 (Westin), R21MH116352 (Ning), NARSAD Young Investigator Award (Cetin-Karayumak), K24 MH110807 and R01MH112748 (Kubicki), VA Merit Award (I01 CX000176-06; Shenton).

None of the authors has conflicts of interest.

References

1. Barch DM, Dowd EC. Goal representations and motivational drive in schizophrenia: the role of prefrontal-striatal interactions. *Schizophr Bull* 2010; **36**(5)**:** 919-934.

2. Basser PJ, Pajevic S, Pierpaoli C, Duda J, Aldroubi A. In vivo fiber tractography using DT-MRI data. *Magn Reson Med* 2000; **44**(4)**:** 625-632.
3. Basser PJ, Pierpaoli C. Microstructural and physiological features of tissues elucidated by quantitative-diffusion-tensor MRI. *J Magn Reson B* 1996; **111**(3)**:** 209-219.
4. Mori S, Crain BJ, Chacko VP, van Zijl PC. Three-dimensional tracking of axonal projections in the brain by magnetic resonance imaging. *Annals of neurology* 1999; **45**(2)**:** 265-269.
5. Westin CF, Maier, S.E., Khidhir, B., Everett, P., Jolesz, F.A., Kikinis, R.,. Image processing for diffusion tensor magnetic resonance imaging. *International Conference on Medical Image Computing and Computer-Assisted Intervention*. Springer1999, pp 441-452.
6. Levitt JJ, Zhang F, Vangel M, Nestor PG, Rathi Y, Kubicki M *et al.* The Organization of Frontostriatal Brain Wiring in Healthy Subjects Using a Novel Diffusion Imaging Fiber Cluster Analysis. *Cereb Cortex* 2021; **31**(12)**:** 5308-5318.
7. Kandel E, Schwartz J, Jessell T. *Principles of neural science*. McGraw-Hill, Health Professions Division; New York2000.
8. Murray RM, Lewis SW. Is schizophrenia a neurodevelopmental disorder? *Br Med J (Clin Res Ed)* 1987; **295**(6600)**:** 681-682.
9. Ripke S, Sanders AR, Kendler KS, Levinson DF, Sklar P, Holmans PA *et al.* Genome-wide association study identifies five new schizophrenia loci. *Nature genetics* 2011; **43**(10)**:** 969.
10. Sekar A, Bialas AR, de Rivera H, Davis A, Hammond TR, Kamitaki N *et al.* Schizophrenia risk from complex variation of complement component 4. *Nature* 2016; **530**(7589)**:** 177-183.
11. Weinberger DR. Implications of normal brain development for the pathogenesis of schizophrenia. *Arch Gen Psychiatry* 1987; **44**(7)**:** 660-669.
12. Cronenwett WJ, Csernansky JG. Diving deep into white matter to improve our understanding of the pathophysiology of schizophrenia. *Biol Psychiatry* 2013; **74**(6)**:** 396-397.
13. Friston KJ, Frith CD, Liddle PF, Frackowiak RS. Functional connectivity: the principal-component analysis of large (PET) data sets. *J Cereb Blood Flow Metab* 1993; **13**(1)**:** 5-14.
14. Calhoun VD, Eichele T, Pearlson G. Functional brain networks in schizophrenia: a review. *Front Hum Neurosci* 2009; **3:** 17.
15. Skudlarski P, Jagannathan K, Anderson K, Stevens MC, Calhoun VD, Skudlarska BA *et al.* Brain connectivity is not only lower but different in schizophrenia: a combined anatomical and functional approach. *Biol Psychiatry* 2010; **68**(1)**:** 61-69.
16. Gold JM, Waltz JA, Prentice KJ, Morris SE, Heerey EA. Reward processing in schizophrenia: a deficit in the representation of value. *Schizophr Bull* 2008; **34**(5)**:** 835-847.
17. Levitt JJ, Nestor PG, Levin L, Pelavin P, Lin P, Kubicki M *et al.* Reduced Structural Connectivity in Frontostriatal White Matter Tracts in the Associative Loop in Schizophrenia. *Am J Psychiatry* 2017; **174**(11)**:** 1102-1111.

18. Alexander GE, Crutcher MD. Functional architecture of basal ganglia circuits: neural substrates of parallel processing. *Trends Neurosci* 1990; **13**(7)**:** 266-271.
19. Haber SN. The primate basal ganglia: parallel and integrative networks. *Journal of chemical neuroanatomy* 2003; **26**(4)**:** 317-330.
20. Redgrave P, Rodriguez M, Smith Y, Rodriguez-Oroz MC, Lehericy S, Bergman H *et al.* Goal-directed and habitual control in the basal ganglia: implications for Parkinson's disease. *Nature reviews* 2010; **11**(11)**:** 760-772.
21. Averbeck BB, Lehman J, Jacobson M, Haber SN. Estimates of projection overlap and zones of convergence within frontal-striatal circuits. *J Neurosci* 2014; **34**(29)**:** 9497-9505.
22. Draganski B, Kherif F, Kloppel S, Cook PA, Alexander DC, Parker GJ *et al.* Evidence for segregated and integrative connectivity patterns in the human Basal Ganglia. *J Neurosci* 2008; **28**(28)**:** 7143-7152.
23. Lehericy S, Ducros M, Van de Moortele PF, Francois C, Thivard L, Poupon C *et al.* Diffusion tensor fiber tracking shows distinct corticostriatal circuits in humans. *Annals of neurology* 2004; **55**(4)**:** 522-529.
24. Haber SN. Convergence of Limbic, Cognitive, and Motor Cortico-Striatal Circuits with Dopamine Pathways in Primate Brain. In: Iversen LL, Iversen SD, Dunnett SB, Bjorklund A (eds). *Dopamine Handbook*. Oxford University Press, Inc.: Oxford, 2010, pp 38-48.
25. Casey BJ, Epstein JN, Buhle J, Liston C, Davidson MC, Tonev ST *et al.* Frontostriatal connectivity and its role in cognitive control in parent-child dyads with ADHD. *Am J Psychiatry* 2007; **164**(11)**:** 1729-1736.
26. Liston C, Malter Cohen M, Teslovich T, Levenson D, Casey BJ. Atypical prefrontal connectivity in attention-deficit/hyperactivity disorder: pathway to disease or pathological end point? *Biol Psychiatry* 2011; **69**(12)**:** 1168-1177.
27. Haas BW, Barnea-Goraly N, Lightbody AA, Patnaik SS, Hoeft F, Hazlett H *et al.* Early white-matter abnormalities of the ventral frontostriatal pathway in fragile X syndrome. *Dev Med Child Neurol* 2009; **51**(8)**:** 593-599.
28. Heller C, Steinmann S, Levitt JJ, Makris N, Antshel KM, Fremont W *et al.* Abnormalities in white matter tracts in the fronto-striatal-thalamic circuit are associated with verbal performance in 22q11.2DS. *Schizophr Res* 2020; **224:** 141-150.
29. Quan M, Lee SH, Kubicki M, Kikinis Z, Rathi Y, Seidman LJ *et al.* White matter tract abnormalities between rostral middle frontal gyrus, inferior frontal gyrus and striatum in first-episode schizophrenia. *Schizophr Res* 2013; **145**(1-3)**:** 1-10.
30. Levitt JJ, Nestor PG, Kubicki M, Lyall AE, Zhang F, Riklin-Raviv T *et al.* Miswiring of Frontostriatal Projections in Schizophrenia. *Schizophr Bull* 2020.
31. Zhang F, Wu Y, Norton I, Rigolo L, Rathi Y, Makris N *et al.* An anatomically curated fiber clustering white matter atlas for consistent white matter tract parcellation across the lifespan. *NeuroImage* 2018; **179:** 429-447.

32. Cetin Karayumak S, Bouix S, Ning L, James A, Crow T, Shenton M *et al.* Retrospective harmonization of multi-site diffusion MRI data acquired with different acquisition parameters. *NeuroImage* 2019; **184:** 180-200.
33. Malcolm JG, Shenton ME, Rathi Y. Filtered multitensor tractography. *IEEE Trans Med Imaging* 2010; **29**(9)**:** 1664-1675.
34. Reddy CP, Rathi Y. Joint Multi-Fiber NODDI Parameter Estimation and Tractography Using the Unscented Information Filter. *Front Neurosci* 2016; **10:** 166.
35. Farquharson S, Tournier JD, Calamante F, Fabinyi G, Schneider-Kolsky M, Jackson GD *et al.* White matter fiber tractography: why we need to move beyond DTI. *Journal of neurosurgery* 2013; **118**(6)**:** 1367-1377.
36. Vos SB, Viergever MA, Leemans A. Multi-fiber tractography visualizations for diffusion MRI data. *PLoS One* 2013; **8**(11)**:** e81453.
37. A Unified Tractography Framework for Comparing Diffusion Models on Clinical Scans. *Proceedings of the In Computational Diffusion MRI Workshop of MICCAI*2012; Nice.
38. Chen Z, Tie Y, Olubiyi O, Zhang F, Mehrtash A, Rigolo L *et al.* Corticospinal tract modeling for neurosurgical planning by tracking through regions of peritumoral edema and crossing fibers using two-tensor unscented Kalman filter tractography. *Int J Comput Assist Radiol Surg* 2016; **11**(8)**:** 1475-1486.
39. Liao R, Ning L, Chen Z, Rigolo L, Gong S, Pasternak O *et al.* Performance of unscented Kalman filter tractography in edema: Analysis of the two-tensor model. *Neuroimage Clin* 2017; **15:** 819-831.
40. O'Donnell LJ, Suter Y, Rigolo L, Kahali P, Zhang F, Norton I *et al.* Automated white matter fiber tract identification in patients with brain tumors. *Neuroimage Clin* 2017; **13:** 138-153.
41. Zhang F, Norton I, Cai W, Song Y, Wells WM, O'Donnell LJ. Comparison between two white matter segmentation strategies: An investigation into white matter segmentation consistency. *IEEE 14th International Symposium on Biomedical Imaging (ISBI 2017)*2017, pp 796–799.
42. Zhang F, Wu Y, Norton I, Rathi Y, Golby AJ, O'Donnell LJ. Test-retest reproducibility of white matter parcellation using diffusion MRI tractography fiber clustering. *Human brain mapping* 2019; **40**(10)**:** 3041-3057.
43. Descoteaux M, Angelino E, Fitzgibbons S, Deriche R. Regularized, fast, and robust analytical Q-ball imaging. *Magn Reson Med* 2007; **58**(3)**:** 497-510.
44. Ning L, Westin CF, Rathi Y. Estimating diffusion propagator and its moments using directional radial basis functions. *IEEE Trans Med Imaging* 2015; **34**(10)**:** 2058-2078.
45. Guevara P, Duclap D, Poupon C, Marrakchi-Kacem L, Fillard P, Le Bihan D *et al.* Automatic fiber bundle segmentation in massive tractography datasets using a multi-subject bundle atlas. *NeuroImage* 2012; **61**(4)**:** 1083-1099.
46. Jin Y, Shi Y, Zhan L, Gutman BA, de Zubicaray GI, McMahon KL *et al.* Automatic clustering of white matter fibers in brain diffusion MRI with an application to genetics. *NeuroImage* 2014; **100:** 75-90.

47. Lefranc S, Roca P, Perrot M, Poupon C, Le Bihan D, Mangin JF *et al.* Groupwise connectivity-based parcellation of the whole human cortical surface using watershed-driven dimension reduction. *Med Image Anal* 2016; **30:** 11-29.
48. Desikan RS, Segonne F, Fischl B, Quinn BT, Dickerson BC, Blacker D *et al.* An automated labeling system for subdividing the human cerebral cortex on MRI scans into gyral based regions of interest. *NeuroImage* 2006; **31**(3)**:** 968-980.
49. van den Heuvel MP, Scholtens LH, de Reus MA, Kahn RS. Associated Microscale Spine Density and Macroscale Connectivity Disruptions in Schizophrenia. *Biol Psychiatry* 2016; **80**(4)**:** 293-301.
50. Weinberger DR. Future of Days Past: Neurodevelopment and Schizophrenia. *Schizophr Bull* 2017; **43**(6)**:** 1164-1168.
51. Goldman-Rakic PS. The corticostriatal fiber system in the rhesus monkey: organization and development. *Prog Brain Res* 1983; **58:** 405-418.
52. Chen SY, Huang PH, Cheng HJ. Disrupted-in-Schizophrenia 1-mediated axon guidance involves TRIO-RAC-PAK small GTPase pathway signaling. *Proc Natl Acad Sci U S A* 2011; **108**(14)**:** 5861-5866.
53. Mukai J, Tamura M, Fenelon K, Rosen AM, Spellman TJ, Kang R *et al.* Molecular substrates of altered axonal growth and brain connectivity in a mouse model of schizophrenia. *Neuron* 2015; **86**(3)**:** 680-695.
54. Solek CM, Farooqi NAI, Brake N, Kesner P, Schohl A, Antel JP *et al.* Early inflammation dysregulates neuronal circuit formation in vivo via upregulation of IL-1beta. *J Neurosci* 2021.
55. Goldman-Rakic PS. Prenatal formation of cortical input and development of cytoarchitectonic compartments in the neostriatum of the rhesus monkey. *J Neurosci* 1981; **1**(7)**:** 721-735.
56. Haber SN. Neuroanatomy of Reward: A View from the Ventral Striatum. In: Gottfried JA (ed). *Neurobiology of Sensation and Reward*. CRC Press: Boca Raton (FL), 2011.
57. Selemon LD, Goldman-Rakic PS. Longitudinal topography and interdigitation of corticostriatal projections in the rhesus monkey. *J Neurosci* 1985; **5**(3)**:** 776-794.
58. Yeterian EH, Van Hoesen GW. Cortico-striate projections in the rhesus monkey: the organization of certain cortico-caudate connections. *Brain Res* 1978; **139**(1)**:** 43-63.
59. Barch DM, Pagliaccio D, Luking K. Mechanisms Underlying Motivational Deficits in Psychopathology: Similarities and Differences in Depression and Schizophrenia. *Curr Top Behav Neurosci* 2016; **27:** 411-449.
60. Haber SN, Behrens TE. The neural network underlying incentive-based learning: implications for interpreting circuit disruptions in psychiatric disorders. *Neuron* 2014; **83**(5)**:** 1019-1039.
61. Uddin LQ. Cognitive and behavioural flexibility: neural mechanisms and clinical considerations. *Nature reviews* 2021; **22**(3)**:** 167-179.
62. Borst JP, Anderson JR. Using model-based functional MRI to locate working memory updates and declarative memory retrievals in the fronto-parietal network. *Proc Natl Acad Sci U S A* 2013; **110**(5)**:** 1628-1633.

63. Aron AR, Robbins TW, Poldrack RA. Inhibition and the right inferior frontal cortex. *Trends in cognitive sciences* 2004; **8**(4)**:** 170-177.
64. Aron AR, Robbins TW, Poldrack RA. Inhibition and the right inferior frontal cortex: one decade on. *Trends in cognitive sciences* 2014; **18**(4)**:** 177-185.
65. Szczepanski SM, Knight RT. Insights into human behavior from lesions to the prefrontal cortex. *Neuron* 2014; **83**(5)**:** 1002-1018.
66. Burgess PWW, H. Rostral Prefrontal cortex (Brodmann Area 10) Metacognition in the Brain. In: Stuss DTKRT (ed). *Principles of Frontal Lobe Function, 2n d edition*. Oxford University Press: New York, 2013, pp 524-544.
67. Butler PD, Hoptman MJ, Smith DV, Ermel JA, Calderone DJ, Lee SH *et al.* Grant Report on Social Reward Learning in Schizophrenia (dagger). *J Psychiatr Brain Sci* 2020; **5**.
68. Green MF. What are the functional consequences of neurocognitive deficits in schizophrenia? *Am J Psychiatry* 1996; **153**(3)**:** 321-330.
69. Kring AM, Gur RE, Blanchard JJ, Horan WP, Reise SP. The Clinical Assessment Interview for Negative Symptoms (CAINS): final development and validation. *Am J Psychiatry* 2013; **170**(2)**:** 165-172.
70. Oliver LD, Hawco C, Homan P, Lee J, Green MF, Gold JM *et al.* Social Cognitive Networks and Social Cognitive Performance Across Individuals With Schizophrenia Spectrum Disorders and Healthy Control Participants. *Biol Psychiatry Cogn Neurosci Neuroimaging* 2021; **6**(12)**:** 1202-1214.
71. Palaniyappan L, Simmonite M, White TP, Liddle EB, Liddle PF. Neural primacy of the salience processing system in schizophrenia. *Neuron* 2013; **79**(4)**:** 814-828.
72. Strauss GP, Waltz JA, Gold JM. A review of reward processing and motivational impairment in schizophrenia. *Schizophr Bull* 2014; **40 Suppl 2:** S107-116.
73. Maier-Hein KH, Neher PF, Houde JC, Cote MA, Garyfallidis E, Zhong J *et al.* The challenge of mapping the human connectome based on diffusion tractography. *Nat Commun* 2017; **8**(1)**:** 1349.
74. Thomas C, Ye FQ, Irfanoglu MO, Modi P, Saleem KS, Leopold DA *et al.* Anatomical accuracy of brain connections derived from diffusion MRI tractography is inherently limited. *Proc Natl Acad Sci U S A* 2014; **111**(46)**:** 16574-16579.
75. Marder SR, Davis JM, Chouinard G. The effects of risperidone on the five dimensions of schizophrenia derived by factor analysis: combined results of the North American trials. *The Journal of clinical psychiatry* 1997; **58**(12)**:** 538-546.

Figures

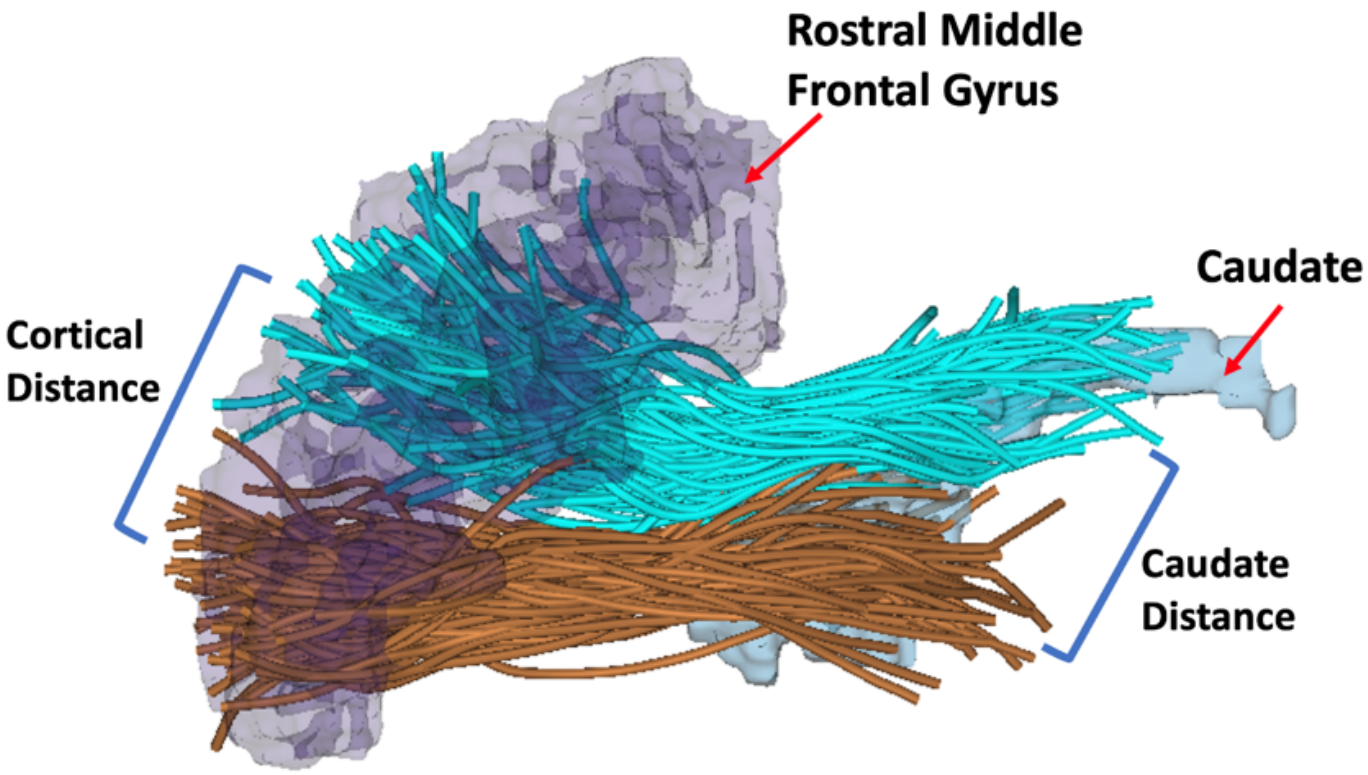

Figure 1

A model of our method for obtaining cortical and caudate mean distances between the endpoints of streamlines of two frontostriatal fiber clusters.

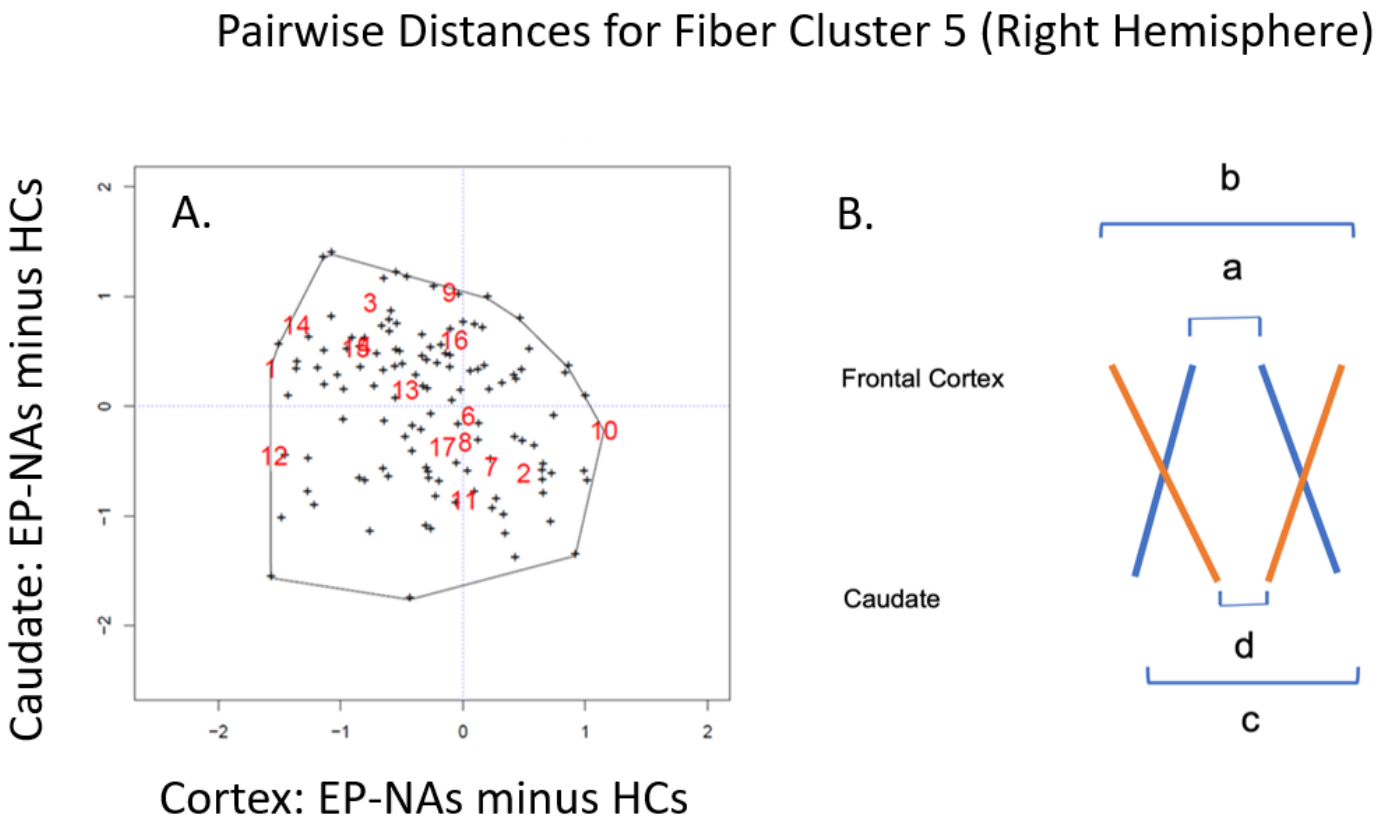

Figure 2

Panel A. shows a plot with a convex hull of the mean difference in cluster endpoint distances (EP-NAs minus HCs) between groups in the right hemisphere. Points (plus signs) and numbers in the upper left quadrant (i.e., -,+ quadrant) show a more convergent pattern in HCs vs EP-NAs. Red numbers, which substitute for a plus sign, label specific cluster pairs for cluster 5. **Panel B.** shows an illustrative example of 2 fiber cluster pairs, one with a more divergent pattern from an EP-NA subject (blue lines) and one with a more convergent pattern from an HC subject (brown lines). Subtracting cluster endpoint distances of an HC subject from an EP-NA subject would result in a point location in the upper left quadrant (i.e., -,+ quadrant) in the plot shown in **Panel A.** More specifically, in this manner, subtracting inter-cluster endpoint distances at the level of the Frontal Cortex (a - b) yields a negative value and subtracting inter-cluster endpoint distances at the level of the Caudate (c - d) yields a positive value. This example yields a data point located in the upper left quadrant (i.e., -,+ quadrant) of the plot shown in **Panel A.** Frontal Cortex represents the origin of the fiber cluster streamline endpoints at the level of the frontal cortex; Caudate represents the termination of the fiber cluster streamline endpoints at the level of the caudate.

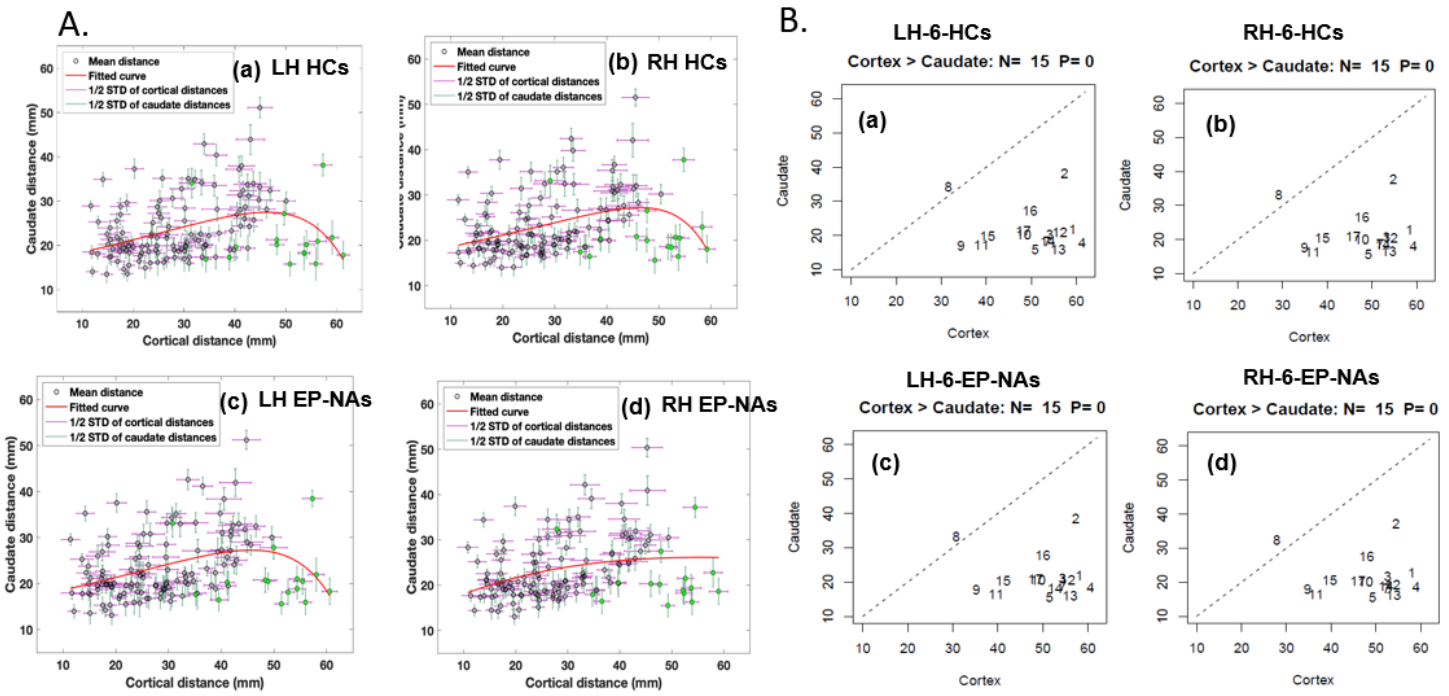

Figure 3

Panel A. Scatter plots showing the relationship between Frontal Cortex (cortical distance) and Caudate inter-cluster endpoint distances in LH HCs (**a**), in RH HCs (**b**), in LH EP-NAs **(c)** and in RH EP-NAs (**d**). Note that the EP-NAs convex curve in the RH (**d**) is more flattened in comparison to the other curves. In **Fig. 3.**, the 16 green circles in each subplot represent clusters that include Cluster 6 as one its cluster pairs. **Panel B.** Plots for Cluster 6 showing the relationship between Frontal Cortex (cortical distance) and Caudate inter-cluster endpoint distances in LH HCs (**a**) and RH HCs (**b**) and LH EP-NAs (**c**) and RH EP-NAs (**d**). We note that the data points in the scatter plots here correspond to the same data points as the green circles in **Fig. 4. Panel A.** See **Fig. S1.** for the scatter plots of all fiber clusters.

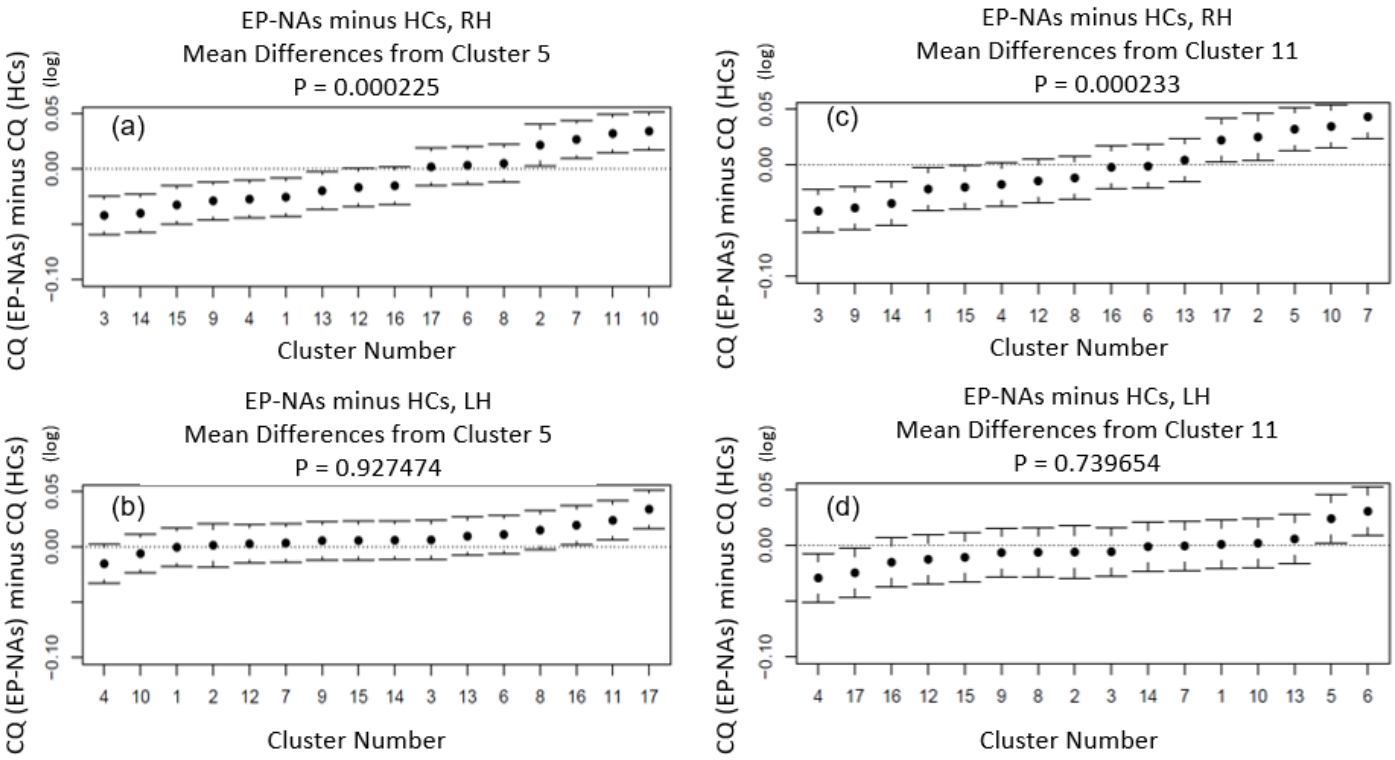

Figure 4

Using a mixed model regression analysis of converge quotients (CQs) for both left and right hemispheres separately, we showed a significant group by fiber cluster pair interaction for RH Cluster 5 (p =.00023) and RH Cluster 11 (p =.00023). We note that fiber cluster 5 originates in the frontal pole and the rostral middle frontal gyrus and fiber cluster 11 originates in the rostral middle frontal gyrus and inferior frontal gyrus, pars orbitalis. (See **Fig. 5.**).

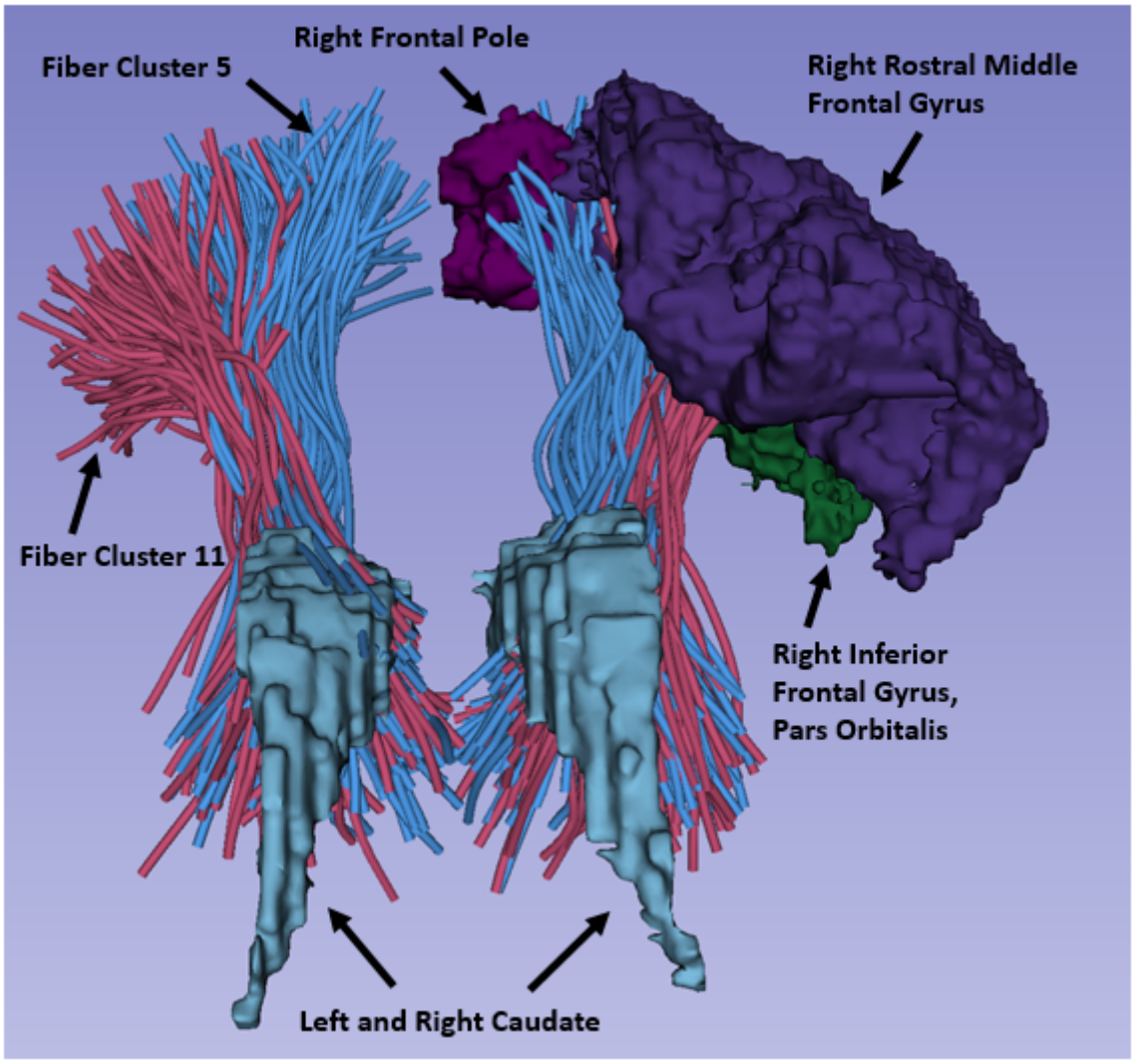

Figure 5

Fiber Clusters 5 and 11 originating in Rostral Middle Frontal Gyrus, Frontal Pole, and Inferior Frontal Gyrus, Pars Orbitalis.

Supplementary Files

This is a list of supplementary files associated with this preprint. Click to download.

- Fig.S1.pdf
- Fig.S2.pdf
- Fig.S3.pdf
- SupplementaryFigureLegends9152022.docx
- SupplementaryTable1.docx